ELSEVIER

J. Non-Newtonian Fluid Mech. 154 (2008) 1–12

Journal of Non-Newtonian Fluid Mechanics

www.elsevier.com/locate/jnnfm

Effects of chemical structures of *para*-halobenzoates on micelle nanostructure, drag reduction and rheological behaviors of dilute CTAC solutions☆

Wu Ge[a], Ellina Kesselman[b], Yeshayahu Talmon[b], David J. Hart[c], Jacques L. Zakin[a,*]

[a] *Department of Chemical and Biomolecular Engineering, The Ohio State University, Columbus, OH 43210, USA*
[b] *Department of Chemical Engineering, Technion-Israel Institute of Technology, Haifa 32000, Israel*
[c] *Department of Chemistry, The Ohio State University, Columbus, OH 43210, USA*

Received 29 October 2006; received in revised form 28 April 2007; accepted 21 January 2008

Abstract

Counterion chemical structure and counterion to cationic surfactant molar ratio, ξ, control counterion binding, micelle nanostructures, drag reduction (DR) effectiveness and rheological behavior of quaternary ammonium surfactant systems. The effects of chemical structures of four sodium *para*-halobenzoate (F, Cl, Br, I) counterions with different ξ values on these properties were compared for dilute solutions of cetyltrimethylammonium chloride (CTAC). Counterion binding was determined by zeta-potential and ^{1}H NMR measurements. Nanostructures were determined by ^{1}H NMR and cryo-TEM imaging. Nanostructures, drag reduction effectiveness measured over a range of temperatures and Reynolds numbers, shear viscosities and first normal stress differences $N1$ were related to the chemical structures of the four counterions and their molar ratios to CTAC.

Micelle nanostructures of the four systems were compared at 30 °C. The *p*-fluorobenzoate system at $\xi = 0.6$ showed no band broadening in ^{1}H NMR spectra and only short threadlike micelle (TLM) structures in cryo-TEM images, was not drag reducing and had zero $N1$. The other halobenzoates had larger TLMs, were DR and viscoelastic at $\xi = 0.6$. The *p*-bromo and *p*-iodobenzoate counterions showed ^{1}H NMR band broadening at $\xi = 0.6$, while the *p*-chlorobenzoate showed band broadening at $\xi = 1.5$. At $\xi = 4.0$, the *p*-fluoro system had small TLMs and no band broadening, was also not drag reducing and had zero $N1$ while the *p*-chloro, *p*-bromo and *p*-iodo systems which contain TLMs and showed band broadening are all DR and have appreciable $N1$.

The *p*-fluoro system also showed only small zeta-potential reductions at all ratios while the other three showed moderate to large decreases in zeta-potential with increase in ξ, crossing from positive to negative values. The ratios at the crossing points followed the order of the molecular size and hydrophobicity: I, Br and Cl.

Keywords: Surfactant drag reduction; Threadlike micelles; Counterion binding; Rheology; Zeta-potential; ^{1}H NMR; Cryo-TEM

1. Introduction

Cationic surfactant systems are known to be drag reducing (DR) when threadlike micelles (TLMs) are present [1–3]. The presence of (or transition to) TLM entanglement results in other unique phenomena such as viscoelasticity [4–8], flow birefringence [9–12] and shear thickening and shear-induced structure (SIS) [13–15]. It is generally believed that organic counterions are required for cationic surfactant molecules to form long, flexible TLMs. DR effectiveness of cationic surfactant/counterion systems, as indicated by the effective temperature, Reynolds number range and critical shear stress for loss of DR, depends on the chemical structure and the molar ratios of counterion to surfactant, ξ [2,16,17]. Substituted benzoates such as salicylate or tosylate are examples of effective TLM promoters. Different techniques such as DR measurements, rheological measurements, NMR, SANS and cryo-TEM are helpful in better understanding the relationships among surfactant and counterion chemical structure, micellar nanostructure and macroscopic behaviors, which would allow one to select or synthesize surfactant additives with appropriate chemical characteristics to

☆ This paper was originally submitted at the PRATO conference.

* Corresponding author. Tel.: +1 614 688 4113; fax: +1 614 292 3769.
E-mail address: zakin.1@osu.edu (J.L. Zakin).

0377-0257/$ – see front matter © 2008 Elsevier B.V. All rights reserved.
doi:10.1016/j.jnnfm.2008.01.011

provide desired turbulent flow properties for specific applications.

Counterions are assumed to be either "free" in the solvent phase or "bound" to the micelles [18]. They are attracted and bound to micelles by two kinds of forces: electrostatic and/or hydrophobic. Due to the dynamic nature of micelles, partial disruption of hydration shells for both surfactant headgroups and counterions, protrusion of part of the surfactant tails from the micelle core into the interface as well as partial hydration of the micelles, counterion binding is very complicated [19,20]. Generally, there are two basic types/locations of binding: interfacial (Stern layer) binding, driven by prevailing electrostatic forces which are predominant for small inorganic counterions such as Cl^-, Br^- and penetrating (micelle core) binding, driven by prevailing hydrophobic forces which are predominant in large organic counterions such as salicylate or naphthoate. While interfacial counterion binding can generally stabilize micelles and lower their CMC to some extent, penetrating counterion binding can greatly promote micellar growth and induce morphological change (spherical to threadlike and further to vesicles) at much lower concentrations [21]. Counterion to surfactant molar concentration ratio, ξ, is an important factor affecting DR ability, rheological properties and nanostructures of DR ionic surfactant solutions [22–25]. With increase in ξ, more counterions bind to the surfactant micelles, either at the micellar surface or penetrating into the micellar interior, changing the net charge on the micelle. The net micellar charge variation can be monitored by zeta-potential, which is measured at the surface of shear and reflects charge effects both from counterions penetrating into the micelle core and adsorbing in the Stern layer.

In this work we discuss how changes in the counterion chemical structure of a series of *p*-halobenzoates and counterion to surfactant ratio affect zeta-potential, nanostructure, DR and rheological properties. The cationic surfactant used was CTAC. Its concentration was fixed at 5 mM, well above its CMC of about 1.3 mM [26] but not high enough to cause any gelation. The organic counterions are four *para*-halobenzoates: F, Cl, Br and I. The widely used sodium salicylate (NaSal) counterion is also included for comparison.

2. Experimental

2.1. Materials studied

CTAC was purchased from Nanjing Robiot Co. Ltd. with a label purity of 99%. *p*-Fluorobenzoic acid (99% purity), *p*-chlorobenzoic acid (99% purity), *p*-bromobenzoic acid (99% purity), *p*-iodobenzoic acid (98% purity) were purchased from Aksci Company. An appropriate amount of NaOH (purchased from Mallinckrodt, AR grade) was used to neutralize each acid. NaSal was purchased from Sigma–Aldrich with a purity of 99%. The concentration of CTAC was 5 mM for all the solutions tested. For zeta-potential measurements, five solutions of about 60 mL were made for each counterion, with molar ratios $\xi = 0.6$, 1, 1.5, 2.5 and 4. Higher ratios were also prepared for the *p*-fluorobenzoate and NaSal sample. In DR measurements, due to the large volume (21 L) needed for each run, the solutions were prepared in a ξ-increasing fashion and each solution (except $\xi = 0.6$, the lowest) was made by adding more counterion to the previous one. All the samples were stirred for 8 h followed by 24 h of rest before measurement except for the cryo-TEM imaging, for which the rest time was much longer (about 3 weeks) due to the international delivery of the samples from Ohio State to the cryo-TEM facility in Israel.

2.2. Drag reduction

Drag reduction was measured in a closed flow loop. The test section was a stainless steel tube with a length of 2.18 m and an inner diameter of 10.9 mm. Flow rate was measured by a Toshiba 8100 magnetic flow meter and pressure drop was measured by a Validyne pressure transducer. The friction factor, f, was calculated from the pressure drop and compared with the friction factor of the solvent (water), f_s, at the same solvent Reynolds number. DR at different temperatures was calculated from Eq. (1) over a solvent Reynolds number range of 3×10^3 to 3×10^5.

$$\mathrm{DR}\% = \frac{f_s - f}{f_s} \times 100 \quad (1)$$

More details on the DR measurements can be found in previous publications [10,27].

2.3. ^1H NMR experiments

^{1}H NMR experiments for the CTAC/Na-*p*-halobenzoate systems in D_2O were performed with a Bruker DRX-600 MHz (14.14 T) NMR spectrometer at the Campus Chemical Instrument Center at The Ohio State University. First, pure counterion ^{1}H NMR spectra of each Na-*p*-halobenzoate were obtained. Then, a series of each counterion was added to a 5 mM CTAC solution. Counterion to surfactant ratios were selected as 0.1, 0.6, 1.5 and 2.5. All NMR samples were prepared following the same stirring and resting procedure described in Section 2.1 and were run in standard NMR tubes at 30 °C.

2.4. Rheological measurements

Shear viscosity, η, and first normal stress difference, $N1$, a measure of viscoelasticity, were measured simultaneously with a 50-mm-diameter cone and plate tool with a cone angle of 0.0204 rad, mounted on an ARES rheometer. With Peltier temperature control (−30 to 150 °C with accuracy of ±0.1 °C), shear viscosity and $N1$ values at 10, 30 and 50 °C were measured using log intervals with 10 points in each decade from 0.1 to 1000 s^{-1} steady rate sweep, with 30 s delay time and 30 s measuring time to ensure equilibrium. $N1$ readings were corrected for inertial effects by a combination of Macosko [28] and water calibration. Only 30 °C data are reported here.

2.5. Zeta-potential measurements

A ZetaPlus zeta-potential analyzer (Brookhaven Instruments Corporation, or BIC) was used to measure zeta-potentials of the

CTAC/Na-*p*-halobenzoate and CTAC/NaSal systems. The Zeta-Plus uses an Electrophoretic Light Scattering (ELS) technique, also known as laser doppler velocimetry (LDV), which is based on reference beam (modulated) optics and a dip-in (Uzgiris type) electrode system to measure the mobility of particles in a known external electric field. With an appropriate model of particle shape chosen, it can calculate zeta-potentials based on mobility information. The claimed accuracy of the instrument is ±2%.

In most cases for surfactant solutions, the Smoluchowski model can be used:

$$\zeta = \frac{\varepsilon}{\mu_e \eta} \tag{2}$$

where ζ = zeta-potential (mV); ε = permittivity of solution (J/(V m)); μ_e = mobility of particle (μ/s)/(V/cm).

2.6. Cryo-TEM

Cryo-TEM images were taken at Technion-Israel Institute of Technology. Cryo-TEM sample preparation was conducted in a temperature-controlled chamber at 30 °C and 100% relative humidity. A small drop of the studied solution was applied on a perforated carbon film supported by an electron microscope grid. The drop was then blotted with filter paper into thin films with thickness of 100–300 nm, and plunged into liquid ethane at its freezing point (~90 K). The process was rapid enough to vitrify the liquid. Images of the vitrified sample were taken and recorded at objective lens underfocus of about 2 μm with an FEI T12 G^2 transmission electron microscope operated at 120 kV, using a Gatan 626 cooling holder operated at about −180 °C. The technique is described in [29].

Cryo-TEM images of the four CTAC/Na-*p*-halobenzoate systems were taken at $\xi = 0.6$ and 4 at 30 °C to identify the effects of both counterion chemical structure and counterion to surfactant molar ratio ξ.

3. Results and discussion

3.1. Zeta-potentials

Fig. 1 shows the measured zeta-potentials of the CTAC/Na-*p*-halobenzoate systems and the CTAC/NaSal system. The CTAC/NaSal system was included in the measurements because NaSal has been extensively studied and is recognized as a very effective counterion to promote cationic surfactant micellar growth [30–33] and CTAC/NaSal is a very good drag reducer [34]. Imae and Kohsaka observed negative zeta-potentials for a tetradecyltrimethylammonium/Sal system at $\xi \approx 4$ [32]. Later Cassidy and Warr measured zeta-potentials and surface potentials on a CTAB/NaSal system and observed negative zeta-potentials at $\xi \approx 4$ but positive surface potential for ξ up to 100 [35]. The former indicates the charge at the shear plane, the latter at the micelle surface. Based on their results, Imae and Kohsaka proposed a *two-site* binding model. Aromatic counterions such as salicylates or naphthoates can both penetrate into the micellar interior and adsorb onto the micellar interface. Fig. 2 is a schematic diagram of the CTAC/Na-*p*-halobenzoate micellar surface based on their model. It shows two binding sites for the benzoate counterions. Several authors [35–37] found that penetrating organic counterions bind to the cationic micelles so strongly that they dominate in the competition for binding to micelles over non-penetrating small counterions such as bromide or chloride. No inorganic counterions have been reported to induce net charge reversal.

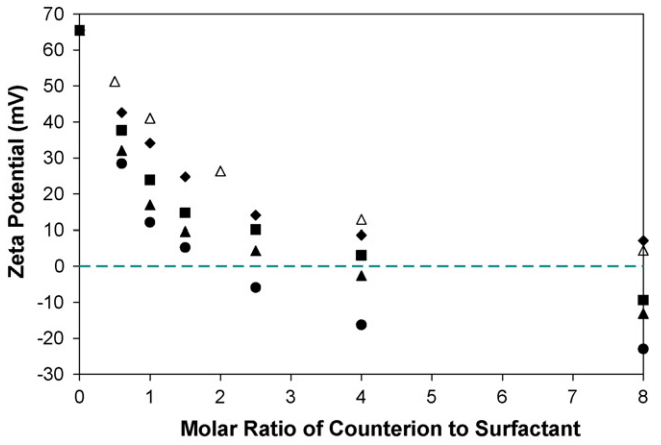

Fig. 1. Zeta-potentials vs. counterion to surfactant molar ratio ξ of CTAC/Na-*p*-halobenzoate systems ($\xi = 0.6, 1, 1.5, 2.5, 4, 8$) and CTAC/NaSal system ($\xi = 0.5, 1, 2, 4, 8$) at 25 °C. (△) CTAC/NaSal; (♦) CTAC/Na-*p*-fluorobenzoate; (■) CTAC/Na-*p*-chlorobenzoate; (▲) CTAC/Na-*p*-bromobenzoate; (●) CTAC/Na-*p*-iodobenzoate. CTAC concentration is 5 mM in all the samples.

The degree of binding (fraction of charges of micellized univalent surfactant ions neutralized by micelle-bound univalent counterions, denoted as β) was reported to be 60% for a CTAC solution at about 5 mM using NMR spectroscopy analysis [38]. For the CTAC/Na-*p*-halobenzoate systems at 5 mM CTAC concentration, β values can be determined by the zeta-potential changes as shown below.

Assume ζ_{CTA+} is the zeta-potential for the micelle contributed solely from the CTA+ cations in the micelle, then for the CTA+/counterions system with a zeta-potential of ζ, its degree of binding is

$$\beta = \frac{\zeta_{CTA+} - \zeta}{\zeta_{CTA+}} \tag{3}$$

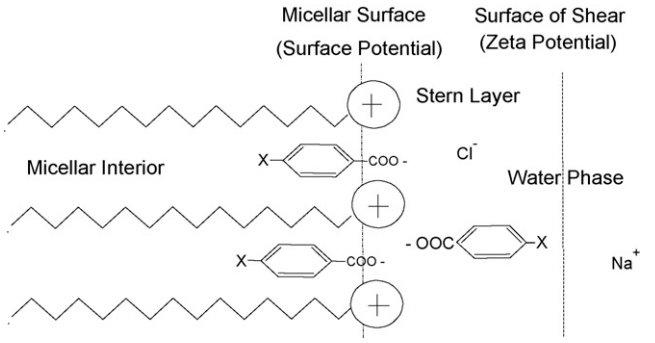

Fig. 2. Schematic diagram of the CTAC/Na-*p*-halobenzoate micellar surface, showing two sites of binding for the aromatic counterions: surface adsorption in the Stern layer and penetrating binding in the micellar interior.

Table 1
Degree of binding, β, at different counterion to surfactant ratios, ξ, for the four CTAC/Na-*p*-halobenzoate systems derived from zeta-potential measurements at 25 °C

ξ	0	0.6	1	1.5	2.5	4	8
p-Fluo	0.60	0.74	0.79	0.85	0.91	0.95	0.96
p-Chloro	0.60	0.77	0.85	0.91	0.94	0.98	1.06
p-Bromo	0.60	0.80	0.90	0.94	0.97	1.02	1.08
p-Iodo	0.60	0.83	0.93	0.97	1.04	1.10	1.14

when $\xi = 0$, the zeta-potential of 5 mM CTAC is 65 mV (see Fig. 1) and the degree of binding is 0.6 [38]. From Eq. (3), $\zeta_{CTA+} = 162.5$ mV, giving

$$\beta = \frac{162.5 - \zeta}{162.5} \quad (4)$$

β values obtained from ζ values in Fig. 1 and Eq. (4) are listed in Table 1. Note that when β values exceed 1, an alternative definition of β is needed. Here β is the ratio of univalent micelle-bound counterion concentration to the micellized concentration of surfactant ions.

In the systems investigated, neither the CTAC/NaSal nor the CTAC/Na-*p*-fluorobenzoate systems show net charge reversal for ξ up to 8. However, above about $\xi = 11$, ζ for the NaSal system reverses charge and becomes negative. The zeta-potential curve for the CTAC/Na-*p*-fluorobenzoate system flattens out at ξ above 4 with little change when ξ increases to 20. Cassidy and Warr, with much higher surfactant concentration (25 mM) [35], observed net charge reversal in their CTAB/NaSal system at $\xi \approx 4$. On the other hand, Na-*p*-chlorobenzoate, Na-*p*-bromobenzoate and Na-*p*-iodobenzoate all caused net charge reversal, at $\xi \approx 5$, 3.5 and 2, respectively and showed no flattening out in the ξ range investigated.

From Table 1 it is seen that the degree of binding for the four CTAC/Na-*p*-halobenzoate systems increases in the order F, Cl, Br and I. This is also the order of the hydrophobicity of the counterions, which favors penetration binding. It is difficult to explain the negative zeta-potential without proposing that an excess of the more hydrophobic counterions (*p*-iodo, *p*-bromo and *p*-chloro) penetrate into the micelles. Measurements of micelle surface charge are needed to test this hypothesis.

3.2. ^1H NMR

Figs. 3–6 show the ^{1}H NMR ring proton chemical shift results for the four CTAC/Na-*p*-halobenzoate systems in D_2O at 30 °C. In each figure, the bottom spectrum is for the pure counterion and the upper spectra are for $\xi = 0.1$, 0.6, 1.5 and 2.5. Assignments of ring protons for *p*-fluoro, *p*-chloro and *p*-bromobenzoates were based on a combination of reported *p*-halobenzoic acid standard ^{1}H NMR spectra [39] and the observation that protons penetrating into the micelle interior shift upfield and protons nearer the charged headgroups shift downfield relative to the counterion alone in D_2O [4,5,40]. Ring protons for the *p*-iodobenzoate were assigned by extrapolating the trends in chemical shift changes observed for the *p*-fluoro, *p*-chloro and *p*-bromobenzoates, and once again, the chemical

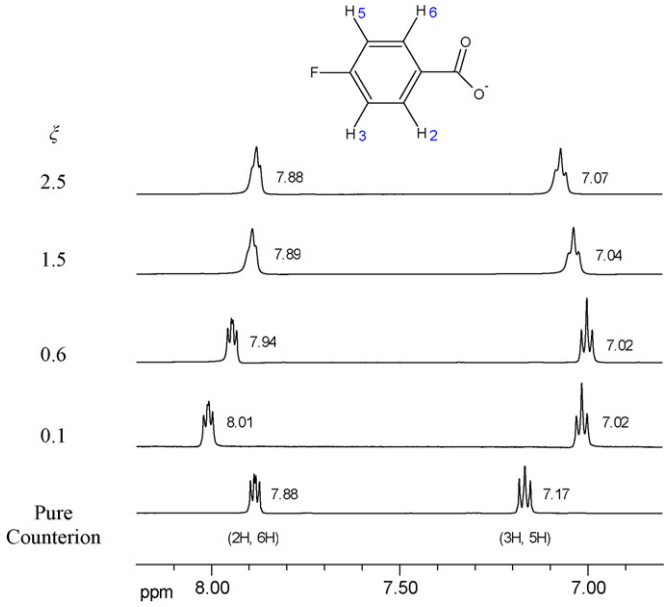

Fig. 3. Ring proton chemical shifts in ^{1}H NMR spectra for CTAC/Na-*p*-fluorobenzoate systems in D_2O at 30 °C. ξ denotes counterion to surfactant molar ratio. The bottom spectrum is the pure counterion Na-*p*-fluorobenzoate in D_2O. From bottom up, 0.5, 3, 7.5 and 12.5 mM Na-*p*-fluorobenzoate was added to a 5 mM CTAC solution.

shift changes observed upon their penetration into the micelles. We note that our assignments of 2H, 6H and 3H, 5H are reversed from those reported previously [39]. Different resonance peak positions were observed among the four pure counterions. The chemical shift of 2H and 6H decreases and 3H and 5H increases, as the *para*-substitution changes from F to Cl, Br and I, finally crossing over at I. This change is attributed to the change in

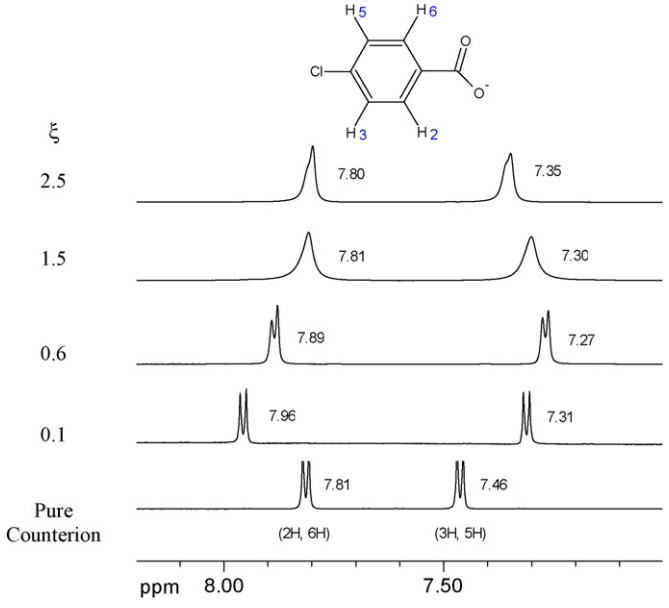

Fig. 4. Ring proton chemical shifts in ^{1}H NMR spectra for CTAC/Na-*p*-chlorobenzoate systems in D_2O at 30 °C. ξ denotes counterion to surfactant molar ratio. The bottom spectrum is the pure counterion Na-*p*-chlorobenzoate in D_2O. From bottom up, 0.5, 3, 7.5 and 12.5 mM Na-*p*-chlorobenzoate was added to a 5 mM CTAC solution.

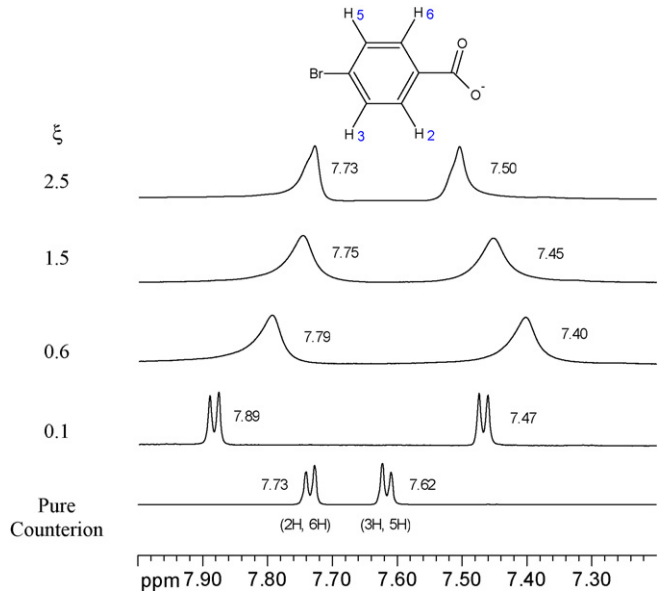

Fig. 5. Ring proton chemical shifts in ^{1}H NMR spectra for CTAC/Na-*p*-bromobenzoate systems in D_2O at 30 °C. ξ denotes counterion to surfactant molar ratio. The bottom spectrum is the pure counterion Na-*p*-bromobenzoate in D_2O. From bottom up, 0.5, 3, 7.5 and 12.5 mM Na-*p*-bromobenzoate was added to a 5 mM CTAC solution.

electronic environment on the ring by the different halogens. All four halogens are strong electron withdrawers through the σ bond (inductive-withdrawal). However, the ability of halogens to supply electrons to the benzene ring (resonance-donation) increases as their size decreases from I to Br to Cl to F. Thus, the protons ortho to the halogen (3H and 5H) are much further upfield for the *p*-fluorobenzoate than for the other halogenated benzoates.

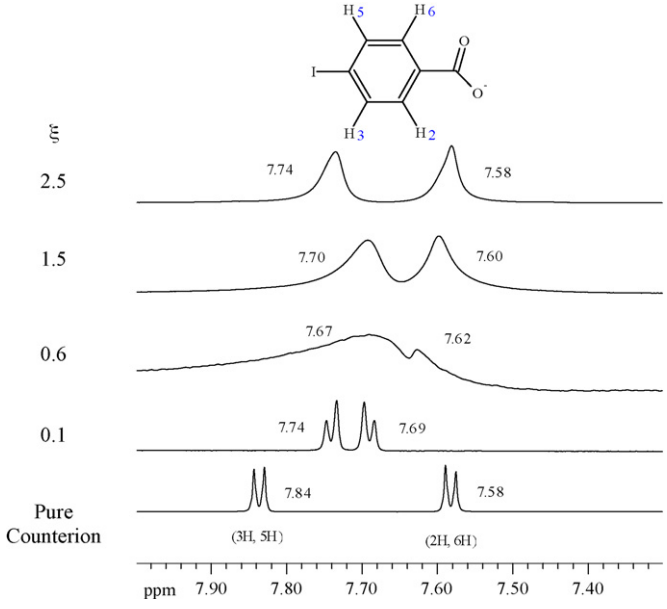

Fig. 6. Ring proton chemical shifts in ^{1}H NMR spectra for CTAC/Na-*p*-iodobenzoate systems in D_2O at 30 °C. ξ denotes counterion to surfactant molar ratio. The bottom spectrum is the pure counterion Na-*p*-iodobenzoate in D_2O. From bottom up, 0.5, 3, 7.5 and 12.5 mM Na-*p*-iodobenzoate was added to a 5 mM CTAC solution.

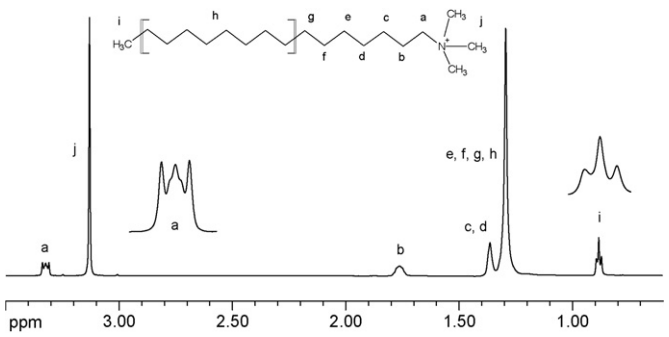

Fig. 7. ^{1}H NMR surfactant proton chemical shifts for 5 mM CTAC in D_2O at 30 °C.

For all four CTAC/Na-*p*-halobenzoate systems, 2H and 6H shift downfield (higher ppm) and 3H and 5H shift upfield (lower ppm) when going from pure counterion to the CTAC system at $\xi = 0.1$. This phenomenon has been observed by several researchers and is attributed to the change in environment when the benzoate counterions are transferred from the bulk D_2O phase to the micellar interface with the hydrophobic *p*-halophenyl ring inserted into the less polar micellar interior and the hydrophilic carboxyl group in contact with water [4,5,40,41] and/or the cationic headgroup. This also explains the further (smaller) upfield shifts of about 0.07 ppm for all four sets of 3H and 5H protons when $\xi = 0.1$ is increased to 0.6. The backward shifts when ξ is increased from 0.6 to higher ratios, which have also been observed by other researchers [5,40,41], can be explained by the fact that counterions in the bound and unbound states exchange rapidly and the observed locations of the counterion proton peaks reflect the average of these two environments. With further increase of ξ, there are more unbound, free benzoate counterions in the water and they contribute more to the averaged peak locations, shifting them back in the direction of the pure counterions.

It should also be noted that there is significant band broadening at $\xi = 0.6$ and above for the *p*-bromo and *p*-iodo systems and at $\xi = 1.5$ and above for the *p*-chloro system. This suggests that the rate of "benzoate exchange" (in and out of micelles) or the mobility of the benzoate within micellar structures slows appreciably as one goes from *p*-fluoro to *p*-chloro to *p*-bromo to *p*-iodobenzoate.

In all spectra, 2H and 6H shift back upfield when ξ is increased from 0.1 to 0.6. This cannot be simply explained by taking into account the increasing free counterions in the bulk solution because no downfield shift in the direction of the free counterions is observed for the 3H and 5H protons, nor can this be explained by a possible increase in Stern layer surface binding, because we would expect this to cause 2H and 6H to shift further downfield. Rather, it suggests that the increase in benzoate concentration (and incorporation into micelles) results in a subtle change in micelle structure such that 2H and 6H pass through the positively charged surface region and deeper into the less polar micellar interior. The upfield shifts of 3H and 5H for $\xi = 0.1$ to 0.6 are relatively small because they are already deep in the micellar interior.

Fig. 7 shows the ^{1}H NMR surfactant proton chemical shifts for 5 mM CTAC in D_2O at 30 °C. The chemical shifts were assigned based on a previously reported CTAC spectrum [39] and 2D correlated spectroscopy (COSY) experimental results from Rao et al. [42]. The *a*-protons appear furthest downfield as a multiplet peak ($\delta = 3.32$), adjacent to the *j*-protons peak ($\delta = 3.13$). Moving upfield, *b*-protons appear as a broad signal ($\delta = 1.77$), followed by a peak representing protons *c* and *d* ($\delta = 1.37$). In the pure CTAC spectrum, protons *e* through *h* are indistinguishable and are grouped together as a single peak at $\delta = 1.28$. The *i*-protons appear as a triplet peak ($\delta = 0.88$). All these chemical shift assignments were confirmed by integration of the resonance peaks.

Upon addition of Na-*p*-halobenzoate, the chemical shifts of protons *a* through *g* as well as protons *j* shift upfield due to the ring current shielding they experience because of the counterion insertion. Protons *h* and *i*, located further from the headgroup, remain unshifted. Fig. 8 shows the upfield shift of *a*, *j* protons with increase of ξ in the CTAC/Na-*p*-fluorobenzoate system. The other three CTAC/Na-*p*-halobenzoate systems show similar upfield shift patterns. Figs. 9 and 10 show the upfield protons ($b-i$) for the four CTAC/Na-*p*-halobenzoate systems at two ξ values, 0.1 and 0.6. At $\xi = 0.1$, the influence of the inserted *p*-halophenyl rings is to shift the *b*-protons about 0.07 ppm upfield for all four systems. The *c*, *d*-protons are also shifted upfield such that they overlap with the *e to h* peak. This represents a relatively shallow net *p*-halobenzoate penetration depth wherein 2H and 6H of the *p*-halophenyl rings lie near the micellar surface and experience the full influence of the polar headgroups, resulting in a significant downfield shift of these signals in the ^{1}H NMR spectra as shown in Figs. 3–6. When ξ is increased to 0.6, there is a significant upfield shift for 2H and 6H (relative to $\xi = 0.1$), suggesting that the net penetration of the *p*-halophenyl rings is deeper into the micelle (Figs. 3–6). This increase in *p*-halobenzoate concentration also affects CTAC protons *a* to *g* and *j*, which also shift upfield. Chemical shift assignments at $\xi = 0.6$ were based in part on a COSY experimental result from Kreke et al. [43] and supported by integration of the resonance peaks.

The magnitude of the chemical shift change for protons *a*, *b*, *c* and *d* is approximately the same for the four *p*-halophenyl counterions at $\xi = 0.1$, indicating that they penetrate to about the same depth into the micellar interior (see Fig. 9). However, at $\xi = 0.6$, there is an increase in the upfield shifts of *b*, *c*, *d*, *e* and even *f* going from *p*-fluoro to *p*-chloro (see Fig. 10). Because of band broadening, it is difficult to assign locations for these protons in the *p*-bromo and *p*-iodo systems, but the *p*-bromo protons appear to follow this trend.

The increasing influence of the larger halogen counterions into the hydrocarbon core of the micelles may be related to their increasing size or their increasing hydrophobicity. Because of the insertion of these counterions, the effective volume, *v*, of the hydrocarbon chain in the micelles is enlarged, resulting in larger packing parameter $p = v/a_0 l_c$ [44], assuming that the optimal head group area a_0 and critical chain length l_c remain roughly unchanged. The molecular volume of these four counterions increases significantly in the order of F, Cl, Br and I, therefore, the packing parameter *p* increases in the same order, resulting in the promotion and growth of longer TLMs. Recently, Geng et al. proposed an interfacial specific ion-pairing/hydration model suggesting that specific ion-pairing and interfacial hydration are the controlling factors in TLM formation and elongation for cationic micelles with aromatic counterions [20,45]. According to this model, increasing polarizability and associated free energy of dehydration going from fluoride to iodide leads to an increase in their degree of binding and concomitantly, an increase in the amount of dehydration from the interfacial region, contributing to tighter packing.

The CTAC line widths of the *p*-bromo and *p*-iodo systems dramatically broadened at $\xi = 0.6$ (see Fig. 10). This can also be seen in the ring protons spectra where the *p*-fluoro peaks do not broaden at all concentrations (Fig. 3) but the *p*-bromo and *p*-iodo systems show significant band broadening starting at $\xi = 0.6$ (Figs. 5 and 6) and *p*-chloro at $\xi = 1.5$ (Fig. 4). The band broadening in these systems is attributed to inhibition of the end-over-end tumbling motion of TLMs [4] due to formation of large TLMs in the *p*-chloro, *p*-bromo and *p*-iodo systems which grow longer and more flexible with increase in ξ.

3.3. Cryo-TEM

Fig. 11 shows cryo-TEM images for the four CTAC/Na-*p*-halobenzoate systems. $\xi = 0.6$ in the left column. $\xi = 4$ in the right column. From top to bottom the images are CTAC/Na-*p*-fluorobenzoate, CTAC/Na-*p*-chlorobenzoate, CTAC/Na-*p*-bromobenzoate and CTAC/Na-*p*-iodobenzoate.

In the CTAC/Na-*p*-fluorobenzoate images, there are only spherical micelles at $\xi = 0.6$. At $\xi = 4$, in addition to the spheres, there are some short TLMs. This is consistent with the observations that this system has low viscosity, no viscoelasticity, shows no ^{1}H NMR band broadening and its DR ability is very poor.

The other three systems at $\xi = 4$ all have long TLMs, are viscoelastic and show good DR ability. The TLMs in the CTAC/Na-*p*-chlorobenzoate and the CTAC/Na-*p*-bromobenzoate systems at $\xi = 4$ are stiff and less entangled (larger persistence length) while those in the CTAC/Na-*p*-iodobenzoate systems are flexible and entangled. As shown in the rheology and DR results at $\xi = 4$ in Table 2, the entangled, flexible TLMs of the CTAC/Na-*p*-iodobenzoate system have lower viscosity and viscoelasticity and also lower maximum DR than the bromo and chloro systems. Similar features of flexible TLMs were reported earlier by Zhang [27].

3.4. Shear viscosity and N1

Fig. 12 shows the shear viscosity and $N1$ values for CTAC/Na-*p*-halobenzoate systems at 30 °C at $\xi = 0.6$, 1.5, 2.5 and 4. Subplot (1) is shear viscosity vs. shear rate for CTAC/Na-*p*-iodobenzoate. The CTAC/Na-*p*-chloro and bromobenzoate systems show similar shear viscosity behavior while the CTAC/Na-*p*-fluorobenzoate system had very low viscosities at all values of ξ as would be expected from its predominantly

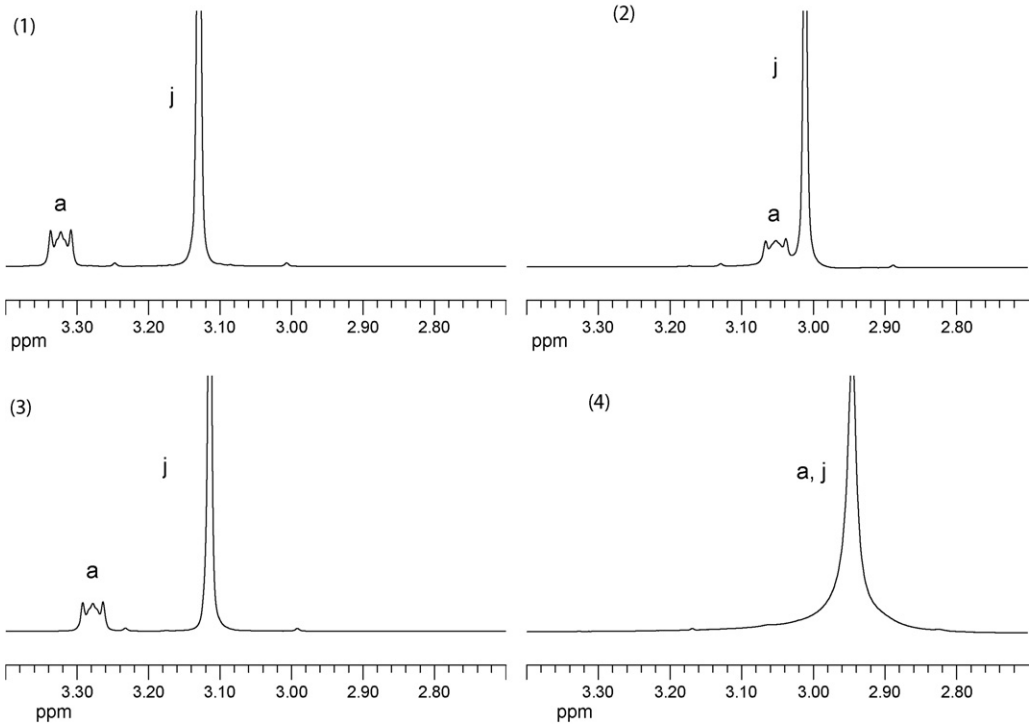

Fig. 8. ^{1}H NMR chemical shifts of *a*, *j* protons for CTAC/Na-*p*-fluorobenzoate systems in D_2O at 30 °C. (1) $\xi = 0$; (2) $\xi = 0.1$; (3) $\xi = 0.6$; (4) $\xi = 1.5$.

spherical and short TLM nanostructures. The other three systems are shear thinning with local maxima indicating shear-induced structure (SIS) at shear rates between 10 and 100 s^{-1} as illustrated in the CTAC/Na-*p*-iodobenzoate data shown.

Subplots (2)–(4) are $N1$ vs. shear rate for the three viscoelastic systems. CTAC/Na-*p*-fluorobenzoate is not viscoelastic and shows zero $N1$ values at all ξ values (data not shown here). From (2) to (4) it is seen that $N1$ values rise rapidly at shear rates

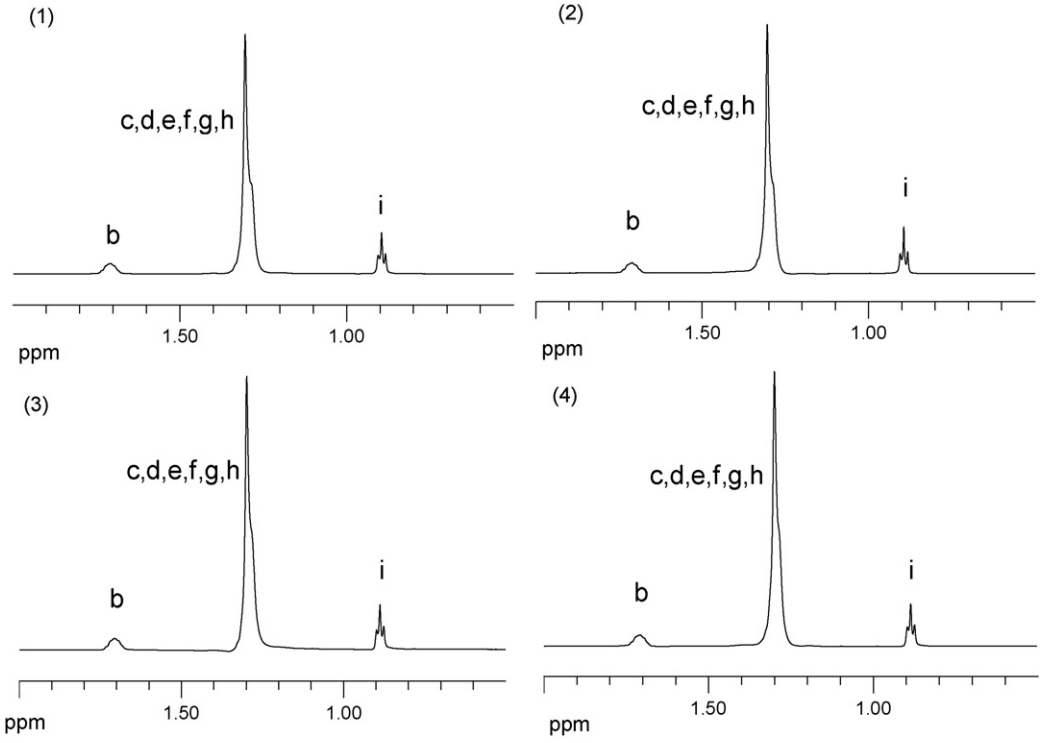

Fig. 9. ^{1}H NMR chemical shifts of *b* to *i* protons for CTAC/Na-*p*-halobenzoate systems in D_2O at $\xi = 0.1$ at 30 °C. (1) CTAC/Na-*p*-fluorobenzoate; (2) CTAC/Na-*p*-chlorobenzoate; (3) CTAC/Na-*p*-bromobenzoate; (4) CTAC/Na-*p*-iodobenzoate.

Table 2
Summary of rheological measurement and drag reduction results for the four CTAC/Na-*p*-halobenzoate systems at 30 °C at $\xi = 0.6$, 1.5, 2.5 and 4

Counterion	ξ	Viscosity at 10 s^{-1} (cp)	Viscosity at 1000 s^{-1} (cp)	Maximum N_1 (Pa)	Maximum %DR	Significant DR temperature range (°C)	Maximum critical wall shear stress (Pa)
p-Fluoro	All	1	1	0	~40	–	–
p-Chloro	0.6	1.4	1.1	33	65	5–30	2
	1.5	18	3.6	470	76	10–55	15
	2.5	22	3.5	320	78	15–62	20
	4	23	4.0	460	79	15–65	28
p-Bromo	0.6	3	2.0	220	74	15–40	10
	1.5	43	4.1	460	77	25–65	20
	2.5	29	4.2	470	80	20–70	30
	4	55	4.1	640	>79	25–75	40
p-Iodo	0.6	15	1.9	100	74	10–55	15
	1.5	17	3.2	340	>77	25–60	30
	2.5	8	2.1	230	>79	20–55	40
	4	20	3.2	400	73	15–65	24

above 10 s^{-1} for $\xi = 4$ and at higher shear rates at lower values of ξ. This is consistent with the occurrence of SIS and the band broadening in the ^{1}H NMR spectra which indicated the formation and growth of TLMs in these systems and is confirmed by their cryo-TEM images.

Numerical summaries of the shear viscosity and $N1$ data are listed in Table 2. It is seen that the three viscoelastic systems all have large $N1$ values at all ξ levels, CTAC/Na-*p*-bromobenzoate has the highest $N1$ values (640 Pa at $\xi = 4$), followed by CTAC/Na-*p*-chlorobenzoate (about 460 Pa at $\xi = 4$) and CTAC/Na-*p*-iodobenzoate (400 Pa at $\xi = 4$). Magnitudes of the shear viscosities also follow the same trend. So in terms of shear viscosity and viscoelasticity from high to low, the series is *p*-bromo, *p*-chloro, *p*-iodo and *p*-fluoro. The lower values of the *p*-iodo's are related to the greater flexibility of their TLMs as noted in Section 3.3.

In the range of shear rates up to 1000 s^{-1}, $N1$ values increases monotonically for the *p*-chloro, *p*-bromo and *p*-iodo systems at $\xi = 0.6$. There is at least one peak in each of the $N1$ curves of $\xi = 1.5$, 2.5 and 4 for these systems, indicating break down or some sort of rearrangement of the TLMs. This is most obvious in $N1$ peaks at $\xi = 2.5$ (denoted as ▲ in Fig. 12) in the CTAC/Na-*p*-chlorobenzoate and CTAC/Na-*p*-iodobenzoate systems, where the $N1$ values increase quickly to about 300 Pa, peak below 1000 s^{-1}, and quickly fall to about 200 Pa before arising again at shear rates above 1000 s^{-1} (not shown in Fig. 12). The TLMs

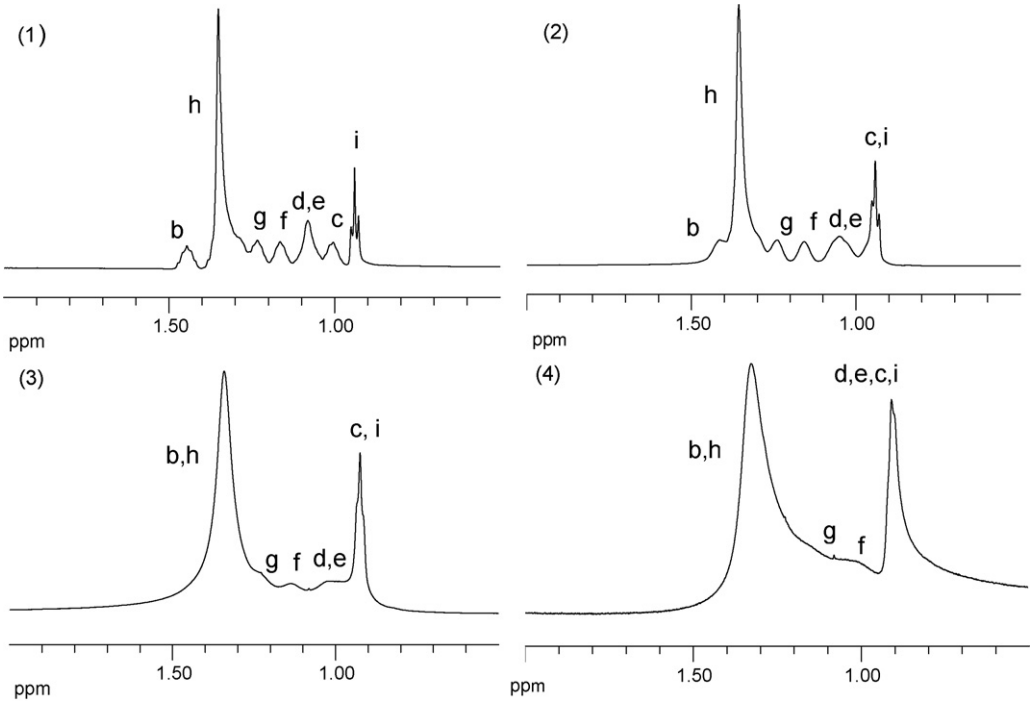

Fig. 10. ^{1}H NMR chemical shifts of *b* to *i* protons for CTAC/Na-*p*-halobenzoate systems in D_2O at $\xi = 0.6$ at 30 °C. (1) CTAC/Na-*p*-fluorobenzoate; (2) CTAC/Na-*p*-chlorobenzoate; (3) CTAC/Na-*p*-bromobenzoate; (4) CTAC/Na-*p*-iodobenzoate.

formed at $\xi = 2.5$ are apparently sensitive to the shear forces which cause shear degradation. New nanostructures apparently form at higher shear levels. Details and explanation of these nanostructure changes are not known.

The viscoelasticity and viscosity of some of the $\xi = 0.6$ systems changed with aging. The data in Table 2 were taken within 48 h of sample preparation while the cryo-TEM images in Fig. 11 were taken several weeks later. The cryo-TEM image of the aged CTAC/Na-*p*-bromobenzoate system at $\xi = 0.6$ in Fig. 11 shows fewer TLMs than the *p*-chloro or *p*-iodo systems although its fresh solution was the most viscoelastic of the three viscoelastic ones at $\xi = 0.6$ (Table 2). The scarcity of TLMs in this solution in the cryo-TEM image taken several weeks after sample preparation coincided with decrease in both its viscosity and viscoelasticity on aging. Viscoelasticity and viscosity of the CTAC/Na-*p*-chlorobenzoate system at $\xi = 0.6$ increased with aging and its cryo-TEM image has well-developed TLMs. There was little change in the properties of the $\xi = 0.6$ CTAC/Na-*p*-iodobenzoate with time, nor with any of the $\xi = 4$ systems [34].

3.5. Drag reduction

Fig. 13 shows selected DR results for the CTAC/Na-*p*-halobenzoate systems. CTAC/Na-*p*-fluorobenzoate does not show significant DR as shown in subplot (1). At very high ξ of 4, it shows modest DR at 10, 15 and 20 °C but practically none above 20 °C as shown in subplot (2). On the other

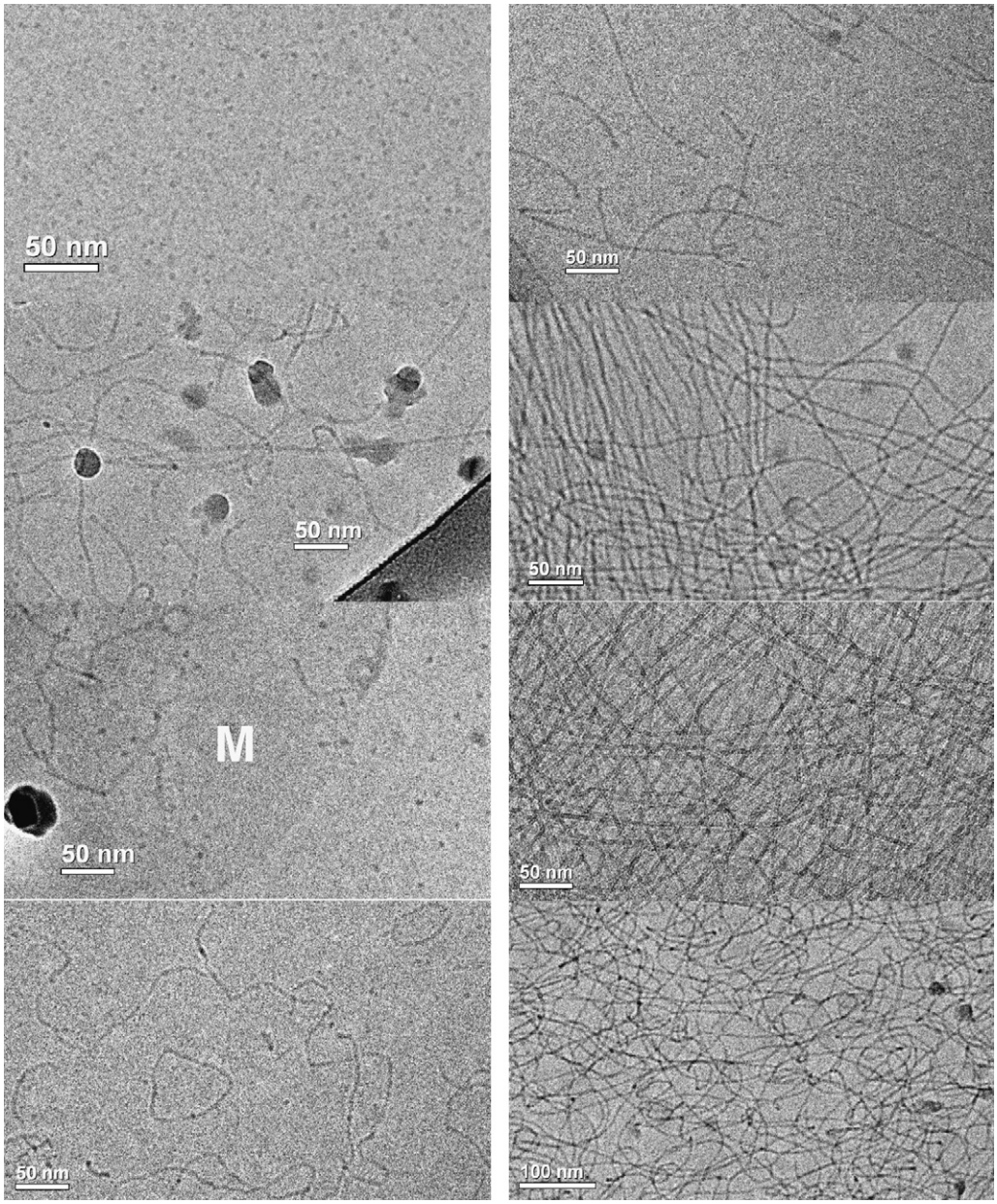

Fig. 11. Cryo-TEM images for the four CTAC/Na-*p*-halobenzoate systems. $\xi = 0.6$ in left column. $\xi = 4$ in right column. From top to bottom: CTAC/Na-*p*-fluorobenzoate, CTAC/Na-*p*-chlorobenzoate, CTAC/Na-*p*-bromobenzoate and CTAC/Na-*p*-iodobenzoate.

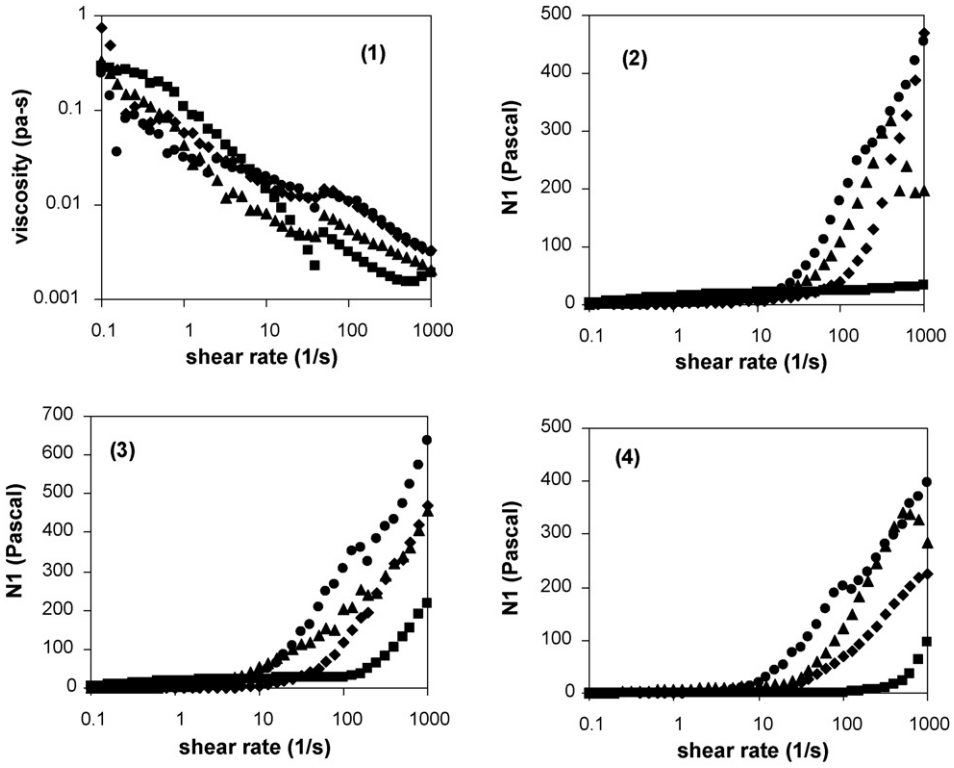

Fig. 12. Shear viscosity and $N1$ values for CTAC/Na-*p*-halobenzoate systems at 30 °C. (1) shear viscosity vs. shear rate for CTAC/Na-*p*-iodobenzoate; (2)–(4) $N1$ vs. shear rate for CTAC/Na-*p*-chlorobenzoate, CTAC/Na-*p*-bromobenzoate, CTAC/Na-*p*-iodobenzoate, respectively. CTAC/Na-*p*-fluorobenzoate is not viscoelastic and has zero $N1$ values (not shown here). (■) $\xi = 0.6$; (♦) $\xi = 1.5$; (▲) $\xi = 2.5$; (●) $\xi = 4$.

hand, CTAC/Na-*p*-iodobenzoate was found to be an effective drag reducer at all the ξ values tested. At $\xi = 0.6$, subplot (3) shows more than 70% average of maximum DR from 10 to 55 °C. All the DR curves at $\xi = 0.6$ peaked in the Reynolds number range tested due to shear degradation of the micelles. Subplot (4) shows even larger maximum DR from 25 to 65 °C for the same system at $\xi = 4$. DR curves at $\xi = 4$ for 45 and 55 °C continue to increase up to the flowrate limit of the test

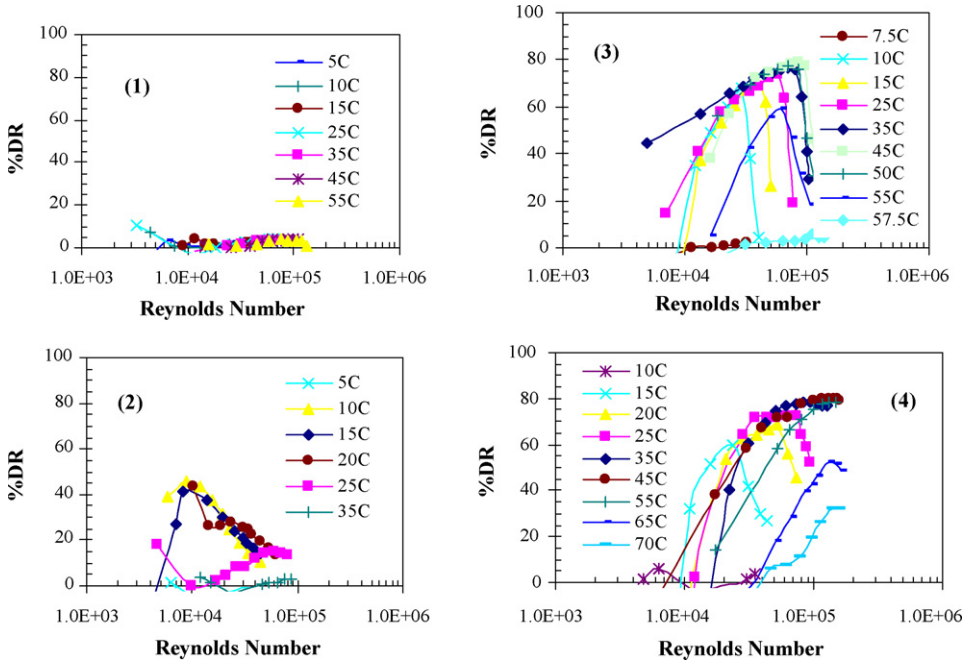

Fig. 13. Drag reduction results for selected CTAC/Na-*p*-halobenzoate systems. (1) CTAC/Na-*p*-fluorobenzoate, $\xi = 0.6$; (2) CTAC/Na-*p*-fluorobenzoate, $\xi = 4$; (3) CTAC/Na-*p*-iodobenzoate, $\xi = 0.6$; (4) CTAC/Na-*p*-iodobenzoate, $\xi = 4$.

system, indicating that the *p*-iodobenzoate TLMs at $\xi = 4$ are both more effective at reducing drag and more robust than at lower ξ values. The CTAC/Na-*p*-chlorobenzoate and CTAC/Na-*p*-bromobenzoate systems $\xi = 4$ show slightly higher maximum DR than CTAC/Na-*p*-iodobenzoate in line with their larger $N1$ and shear viscosity values (see Table 2, where numerical summaries of the rheology and DR results are listed). Critical wall shear stress in the table is the wall shear stress at which the micelles start to break down, causing DR to fall. The temperature range for significant DR is the temperature interval in which DR is greater than 50%. Its lower limit depends on surfactant solubility and the upper limit on the micelles' ability to resist thermal motion. For all three of the halobenzoate systems at all ξ values, there was little difference in the DR behavior at 25 and 35 °C so that comparison with the measured rheological behavior at 30 °C is valid.

4. Conclusions

Changes in counterion chemical structure and in molar ratio to surfactant have dramatic effects on cationic surfactant nanostructure, rheology and drag reduction behavior. Zeta-potential measurements show that the four *para*-substituted benzoate counterions have increasing degrees of binding in accordance with their increasing molecular volume and increase in hydrophobicity and polarizability. Zeta-potentials at high ξ for the chloro, bromo and iodo systems show charge reversal.

The four *p*-halobenzoates penetrate to roughly the same depth into the CTAC micellar interior at $\xi = 0.1$, in spite of their polarizability differences. At $\xi = 0.6$, the influence of *p*-halobenzoate electronic structure on micellar structure as measured by the magnitudes of the shifting of the ^{1}H NMR peaks and band broadening increases in the order F, Cl, Br, and I. This is the same order as the halogen atom size, hydrophobicity and associated free energy of dehydration, leading to increases in packing parameters and to larger more flexible and entangled TLMs as seen in the cryo-TEM images.

While the *p*-chloro, *p*-bromo and *p*-iodo systems are viscoelastic and drag reducing at $\xi = 0.6$, the *p*-fluoro system with spherical micelles shows none of this behavior.

Even at $\xi = 4.0$, the *p*-fluoro system still shows spherical micelles and a few TLMs, with low viscosities, no SIS, no viscoelastic properties ($N1 \approx 0$) and only low levels of drag reduction whereas the other halobenzoates show SIS behavior, have larger viscosities and large $N1$ and are strongly drag reducing reflecting their well-developed TLM nanostructures. For these systems, DR effectiveness as shown by maximum percentage drag reduction is strongly related to viscoelasticity as indicated by $N1$ values.

Acknowledgements

This work was supported in part by the New Energy and Industrial Technology Development Organization (NEDO), Japan. Cryo-TEM imaging was performed at the Hannah and George Krumholz Laboratory for Advanced Electron Microscopy, part of Technion Project on Complex Fluids, Nanostructure and Macromolecules. We also appreciate helpful discussions with Prof. James Rathman and Dr. Ying Zhang.

References

[1] J.L. Zakin, B. Lu, H.-W. Bewersdorff, Surfactant drag reduction, Rev. Chem. Eng. 14 (1998) 253–320.
[2] Y. Qi, J.L. Zakin, Chemical and rheological characterization of drag-reducing cationic surfactant systems, Ind. Eng. Chem. Res. 41 (2002) 6326–6336.
[3] Y. Zhang, J. Schmidt, Y. Talmon, J.L. Zakin, Co-solvent effects on drag reduction, rheological properties and micelle microstructures of cationic surfactants, J. Colloid Interface Sci. 286 (2005) 696–709.
[4] U. Olsson, O. Soederman, P. Guering, Characterization of micellar aggregates in viscoelastic surfactant solutions. A nuclear magnetic resonance and light scattering study, J. Phys. Chem. 90 (1986) 5223–5232.
[5] T. Shikata, H. Hirata, T. Kotaka, Micelle formation of detergent molecules in aqueous media. 2. Role of free salicylate ions on viscoelastic properties of aqueous cetyltrimethylammonium bromide–sodium salicylate solutions, Langmuir 4 (1988) 354–359.
[6] J. Ulmlus, H. Wennerstrom, L.B.-A. Johansson, G. Lindblom, S. Gravsholt, Viscoelasticity in surfactant solutions. Charateristics of the micellar aggregates and the formation of periodic colloidal structures, J. Phys. Chem. 83 (1988) 2232–2236.
[7] J. Myska, J.L. Zakin, Z. Chara, Viscoelasticity of a surfactant and its drag-reducing ability, Appl. Sci. Res. 55 (1996) 297–310.
[8] C. Oelschlaeger, G. Waton, S.J. Candau, Rheological behavior of locally cylindrical micelles in relation to their overall morphology, Langmuir 19 (2003) 10495–10500.
[9] B. C. Smith, Flow birefringence, nuclear magnetic resonance and corrosion measurements on drag-reducing cationic surfactant solutions for district heating and cooling systems, Ph.D. Dissertation, The Ohio State University, 1992.
[10] B. Lu, Characterization of drag reducing surfactant systems by rheology and flow birefringence measurements, Ph.D. Dissertation, The Ohio State University, 1997.
[11] S. Hofmann, P. Stern, J. Myska, Rheological behavior and birefringence investigations on drag-reducing surfactant solutions of tallow-(tris-hydroxyethyl)ammonium acetate/sodium salicylate mixtures, Rheol. Acta 33 (1994) 419–430.
[12] T. Shikata, S.J. Dahman, D.S. Pearson, Rheo-optical behavior of wormlike micelles, Langmuir 10 (1994) 3470–3476.
[13] R. Cressely, V. Hartmann, Rheological behavior and shear thickening exhibited by aqueous CTAB micellar solutions, Eur. Phys. J. B 6 (1998) 57–62.
[14] S. Hofmann, H. Hoffmann, Shear-induced micellar structures in ternary surfactant mixtures: the influence of the structure of the micellar interface, J. Phys. Chem. B 102 (1998) 5614–5624.
[15] Y. Zheng, Z. Lin, J.L. Zakin, Y. Talmon, H.T. Davis, L.E. Scriven, Cryo-TEM imaging the flow-induced transition from vesicles to threadlike micelles, J. Phys. Chem. B 104 (2000) 5263–5271.
[16] B. Lu, X. Li, L.E. Scriven, H.T. Davis, Y. Talmon, J.L. Zakin, Effect of chemical structure on viscoelasticity and extensional viscosity of drag-reducing cationic surfactant solutions, Langmuir 14 (1998) 8–16.
[17] B. Lu, Y. Zheng, H.T. Davis, L.E. Scriven, Y. Talmon, J.L. Zakin, Effect of variations in counterion to surfactant ratio on rheology and microstructures of drag reducing cationic surfactant systems, Rheol. Acta 37 (1998) 528–548.
[18] J.F. Rathman, J.F. Scamehorn, Counterion binding on mixed micelles, J. Phys. Chem. 88 (1984) 5807–5816.
[19] L. Horvath, B. Mihaljevic, V. Tomasic, D. Risovic, N. Filipovic-Vincekovic, Counterion binding to ionic micelles: effects of counterion specificity, J. Dispersion Sci. Technol. 22 (2001) 221–229.
[20] Y. Geng, L.S. Romsted, S. Froehner, D. Zanette, L.J. Magid, I.M. Cuccovia, H. Chaimovich, Origin of the sphere-to-rod transition in cationic micelles with aromatic counterions: specific ion hydration in the interfacial region matters, Langmuir 21 (2005) 562–568.

[21] A.L. Underwood, E.W. Anacker, Organic counterions and micellar parameters: substituent effects in a series of benzoates, J. Phys. Chem. 88 (1984) 2390–2393.
[22] G.D. Rose, K.L. Foster, Drag reduction and rheological properties of cationic viscoelastic surfactant formulations, J. Non-Newtonian Fluid Mech. 31 (1989) 59–85.
[23] B. Lu, Y. Talmon, J.L. Zakin, Effect of counterion to surfactant ratio on rheology and drag reduction behaviors of cationic surfactant systems, Proc. ASME Fluids Eng. Div. 237 (1996) 169–175.
[24] V. Hartmann, R. Cressely, Linear and nonlinear rheology of a wormlike micellar system in presence of sodium tosylate, Rheol. Acta 37 (1998) 115–121.
[25] S.-I. Imai, T. Shikata, Viscoelastic behavior of surfactant threadlike micellar solutions: effect of additives 3, J. Colloid Interface Sci. 244 (2001) 399–404.
[26] P. Mukerjee, K.J. Mysels, Critical Micelle Concentrations of Aqueous Surfactant Systems; Office of Standard Reference Data, National Bureau of Standards, Washington DC, 1971.
[27] Y. Zhang, Correlations among surfactant drag reduction, additive chemical structures, rheological properties and microstructures in water and water/co-solvent systems, Ph. D. Dissertation, The Ohio State University, 2005.
[28] C.W. Macosko, Rheology: principles, measurements, and applications, Wiley–VCH, New York, 1994, p. 550.
[29] Y. Talmon, Cryogenic temperature transmission electron microscopy in the study of surfactant systems, Surfactant Sci. Ser. 83 (1999) 147–178.
[30] J. Ulmius, H. Wennerstroem, L.B.A. Johansson, G. Lindblom, S. Gravsholt, Viscoelasticity in surfactant solutions. Characteristics of the micellar aggregates and the formation of periodic colloidal structures, J. Phys. Chem. 83 (1979) 2232–2236.
[31] T. Shikata, H. Hirata, T. Kotaka, Micelle formation of detergent molecules in aqueous media: viscoelastic properties of aqueous cetyltrimethylammonium bromide solutions, Langmuir 3 (1987) 1081–1086.
[32] T. Imae, T. Kohsaka, Size and electrophoretic mobility of tetradecyltrimethylammonium salicylate (c14tasal) micelles in aqueous media, J. Phys. Chem. 96 (1992) 10030–10035.
[33] H. Rehage, H. Hoffmann, Viscoelastic surfactant solutions: model systems for rheological research, Mol. Phys. 74 (1991) 933–973.
[34] W. Ge, J.L. Zakin, Unpublished work, 2006.
[35] M.A. Cassidy, G.G. Warr, Surface potentials and ion binding in tetradecyltrimethylammonium bromide/sodium salicylate micellar solutions, J. Phys. Chem. 100 (1996) 3237–3240.
[36] H. Rehage, H. Hoffmann, Viscoelastic detergent solutions, Faraday Dis. Chem. Soc. (1983) 363–373.
[37] B.P. Thalody, G.G. Warr, The selective binding of benzoate and hydroxybenzoate ions at cationic surfactant solution/air interfaces, J. Colloid Interface Sci. 175 (1995) 297–303.
[38] B. Lindman, M.C. Puyal, N. Kamenka, R. Rymden, P. Stilbs, Micelle formation of anionic and cationic surfactants from Fourier transform proton and lithium-7 nuclear magnetic resonance and tracer self-diffusion studies, J. Phys. Chem. 88 (1984) 5048–5057.
[39] S.-I. Sasaki, Handbook of Proton-NMR Spectra and Data, Academic Press, Tokyo, Orlando, 1985.
[40] B.C. Smith, L.C. Chou, J.L. Zakin, Measurement of the orientational binding of counterions by nuclear magnetic resonance measurements to predict drag reduction in cationic surfactant micelle solutions, J. Rheol. 38 (1994) 73–83.
[41] Y. Zhang, Y. Qi, J.L. Zakin, Headgroup effect on drag reduction and rheological properties of micellar solutions of quaternary ammonium surfactants, Rheol. Acta 45 (2005) 42–58.
[42] U.R.K. Rao, C. Manohar, B.S. Valaulikar, R.M. Iyer, Micellar chain model for the origin of the visoelasticity in dilute surfactant solutions, J. Phys. Chem. 91 (1987) 3286–3291.
[43] P.J. Kreke, L.J. Magid, J.C. Gee, 1H and 13C NMR studies of mixed counterion, cetyltrimethylammonium bromide/cetyltrimethylammonium dichlorobenzoate, surfactant solutions: the intercalation of aromatic counterions, Langmuir 12 (1996) 699–705.
[44] J.N. Israelachvili (Ed.), Intermolecular and Surface Forces, Academic Press, San Diego, CA, 1991, p. 291.
[45] Y. Geng, L.S. Romsted, F. Menger, Specific ion pairing and interfacial hydration as controlling factors in gemini micelle morphology. Chemical trapping studies, J. Am. Chem. Soc. 128 (2006) 492–501.